Light-Triggered Chemical Biology

DOI: 10.1002/anie.201206698

Control of Nanomolar Interaction and In Situ Assembly of Proteins in Four Dimensions by Light**

*Noemi Labòria, Ralph Wieneke, and Robert Tampé**

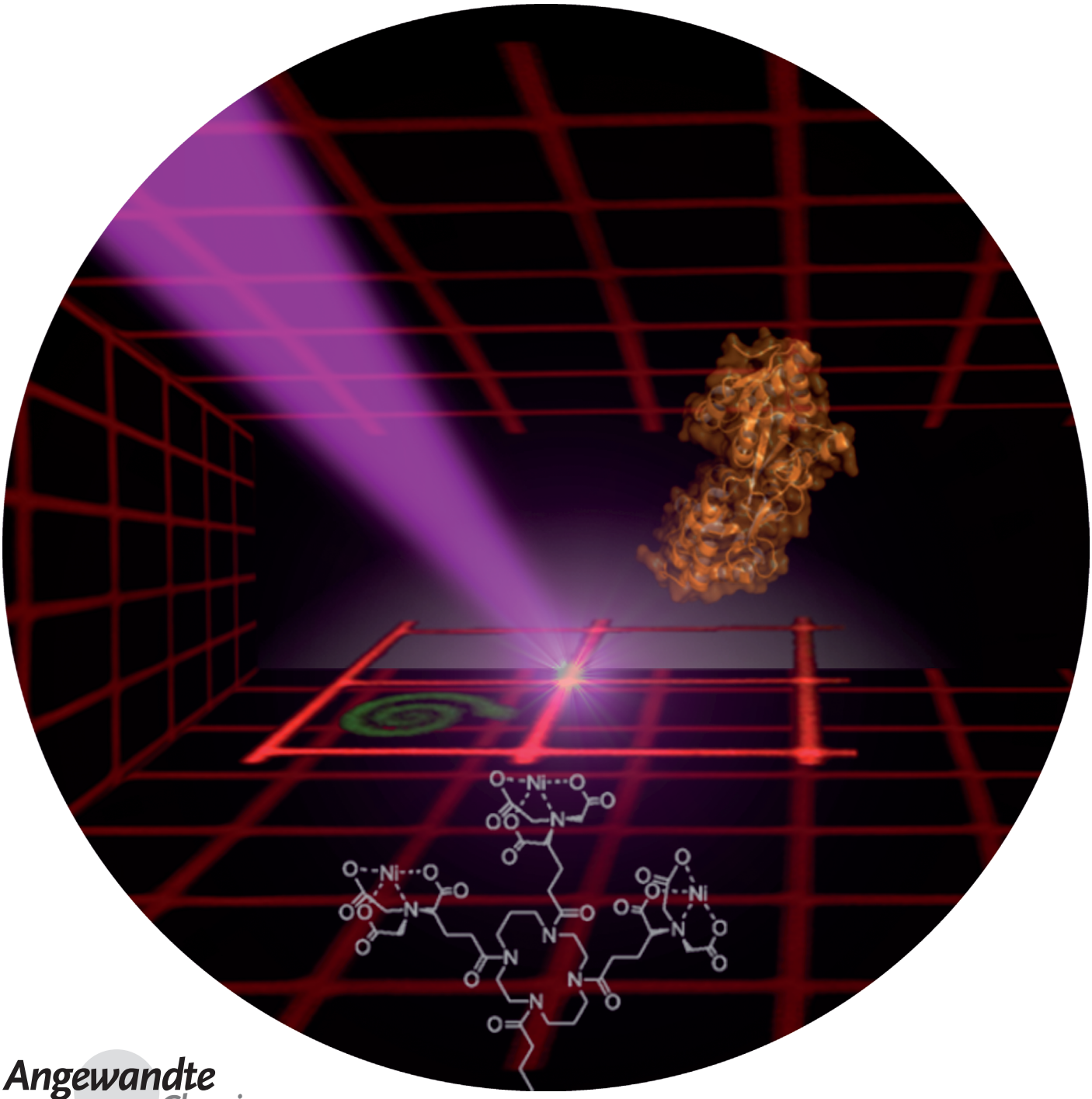

Understanding the function and interaction of cellular components requires efficient methods for labeling, tracking, and assembling proteins.[1] The site-specific incorporation of chemical reporters, such as small organic dyes, genetically encoded fluorescent amino acids,[2] and autofluorescent proteins, highlights these efforts. Traceless modifications with high spatiotemporal control are in high demand to connect protein activity with cellular response. Small fluorescent probes offer a great advantage in terms of visualizing cellular logistics because of their size, superior quantum yield, and photostability. Organic fluorophores are preferred rather than the bulky dimensions of autofluorescent or photoswitchable proteins (> 25 kDa), which can interfere with the protein activity. Light-activatable tools are promising to label, track, and manipulate biomolecules in four dimensions (time and space).[3] Light is compatible with biological samples and can be precisely controlled in time, space, and intensity. In addition, light activation is orthogonal to other chemical reactions. Caged compounds benefit from this feature and are a powerful tool for triggering molecular interactions by light. Myriads of caged and photoactivatable molecules have been described,[4] from the recently reported caged glutathione[5] to genetically encoded photocaged amino acids.[6] This list is continuously increasing, as demonstrated by the plethora of excellent reviews.[7]

The postgenomic era is characterized by considerable efforts being invested in dissecting cellular protein networks, and new strategies are needed to trace proteins of interest (POI) with high spatiotemporal resolution. In the rapidly developing field of chemical biology, tools such as probe incorporation mediated by enzymes (PRIME) and the fusion proteins SNAP-, CLIP-, and Halo-tag have gained renown.[8] Nevertheless, their size (> 20 kDa) does not differ greatly from autofluorescent proteins. The tetracysteine tag,[9] *N*-nitrilotriacetic acid[10] (NTA), or its multivalent derivatives, for example, trisNTA,[11] enable insights into the molecular dynamics, structures, and cellular function of proteins.[12] TrisNTA allows the site-specific and reversible labeling of His-tagged proteins with (sub)nanomolar affinity (K_d = 0.1 nM).[11] His-tagged genomic libraries exist for nearly all organisms and the small size of the trisNTA–His-tag pair does not hamper the structure and function of the protein. In contrast to NTA, trisNTA offers kinetically stable binding ($k_{off} = 0.18\ h^{-1}$), but maintains its reversibility in the presence of imidazole, histidine, and EDTA. This desirable property is of special interest for regeneration in super-resolution microscopy, single-molecule tracking, and sensor applications.[13]

Despite recent progress, a demand for higher spatiotemporal control and resolution for single-molecule and cellular applications as well as high-resolution microscopy still exists. Here, we describe a set of finely tuned photoactivatable trisNTAs (PA-trisNTAs) based on a very small peptidic scaffold that have outstanding autoinhibition and photoactivation properties. Protein interactions were triggered over more than six orders of magnitude and allowed the in situ patterning of proteins in four dimensions.

A series of PA-trisNTAs were designed to achieve (sub-)nanomolar interaction exclusively after photoactivation in a spatiotemporally resolved manner. The general design of PA-trisNTAs is based on the multivalent chelator head trisNTA, which is connected through a peptidic linker to a cumulative histidine sequence (Scheme 1 A). The trisNTA is self-inactivated in the presence of nickel ions through formation of an intramolecular complex. The activation of this small lock-and-key element is ensured by the incorporation of the photocleavable amino acid 3-amino-3-(2-nitrophenyl)propionic acid (Anp). This most commonly used photocleavable amino acid, which readily fragments after exposure to ultraviolet light, is placed at different strategic positions.[14] A single cysteine residue was included close to the N terminus to allow surface immobilization or site-specific labeling with reporter molecules.

The PA-trisNTA **1** with a long linker (11 amino acids) showed moderate self-inactivation in solution as well as on surfaces.[13c] After photoactivation, only 15% of the cleaved trisNTAs binds to His_6-tagged proteins. We followed two strategies to generate a robust self-inactivated trisNTA before activation and a higher binding capacity after light exposure. First, the peptidic linker was adjusted to afford a very compact and tightly autoinhibited complex. Second, by strategically placing the photocleavable amino acid Anp within the self-inactivating histidine residues, an enhanced photoactivation is envisioned as the His-tag is fragmented.

To systematically address these two aspects we applied 9-fluorenylmethoxycarbonyl (Fmoc) solid-phase chemistry to synthesize PA-trisNTAs with different linker lengths and positions of the photocleavable amino acid Anp. Starting with histidine-loaded trityl resins (see the Supporting Information), chain elongation was performed by repetitive cycles of piperidine treatment for cleavage of the Fmoc group and subsequent coupling of the appropriate amino acid by using *O*-(benzotriazol-1-yl)-*N*,*N*,*N*′,*N*′-tetramethyluronium hexafluorophoaphate (HBTU) in the presence of *N*,*N*′-diisopropylethylamine (DIPEA). Afterwards, O*t*Bu-protected trisNTA was introduced at the N terminus through amide bond formation using COMU [(1-cyano-2-ethoxy-2-oxoethylidenaminooxy)dimethylaminomorpholinocarbenium hexafluorophosphate]. Final deprotection and cleavage from the resin was achieved by treatment with trifluoroacetic acid/triisopropylsilane/water/1,2-ethanedithiol/phenol (TFA/TIPS/H_2O/EDT/phenol) for 4 h. After precipitation and purification by RP-C_{18}-HPLC, the identification of all compounds was confirmed by mass spectrometry (see Table S1 in the Supporting Information).

[*] N. Labòria,[+] Dr. R. Wieneke,[+] Prof. R. Tampé
Institut für Biochemie, Biozentrum; Cluster of Excellence Frankfurt
Goethe-Universität Frankfurt
Max-von-Laue-Strasse 9, 60438 Frankfurt/M. (Germany)
E-mail: tampe@em.uni-frankfurt.de
Homepage: http://www.biochem.uni-frankfurt.de

[+] Both authors contributed equally.

[**] This work was supported by the DFG through Ta157/9 (SPP 1623), SFB 902 (B7), as well as ERA-Net-Neuron.

Supporting information for this article is available on the WWW under http://dx.doi.org/10.1002/anie.201206698.

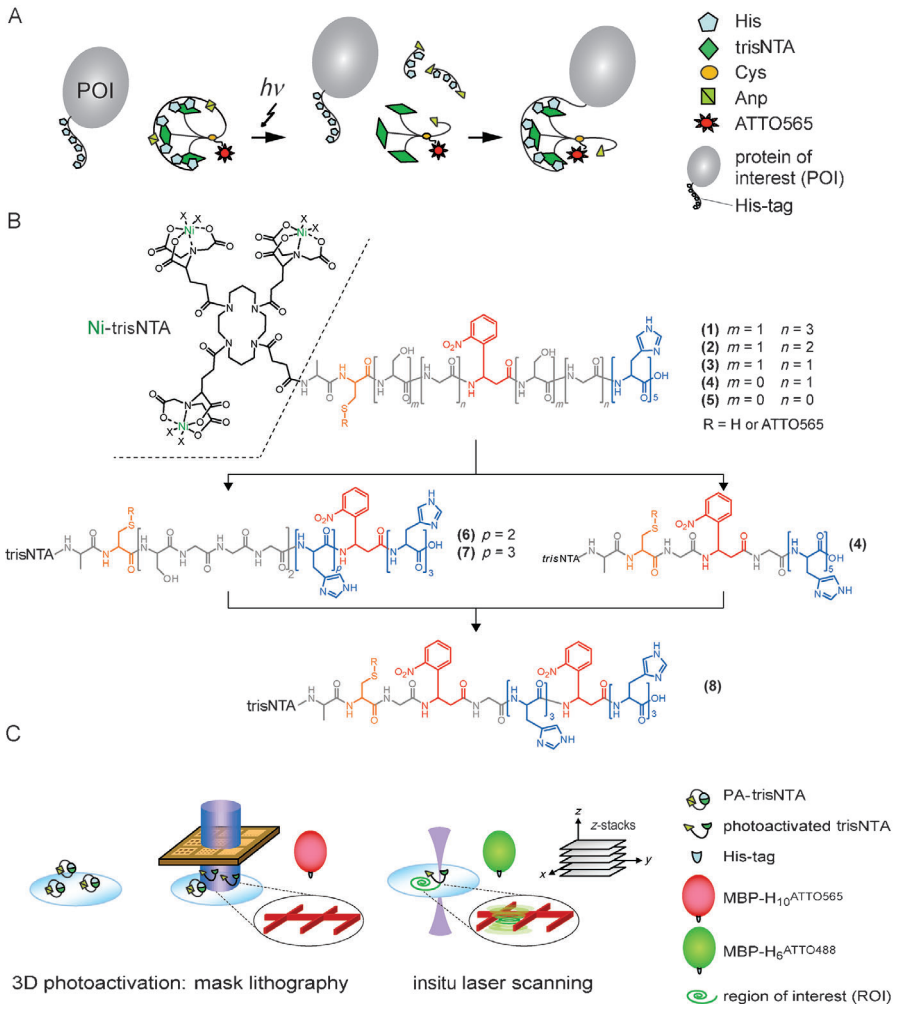

Scheme 1. A) Schematic overview of the PA-trisNTA principle. Based on a very tight autoinhibition, binding between the PA-trisNTA and His-tagged proteins can only occur after photoactivation. B) Chemical structures of the PA-trisNTAs. C) Protein assembly in the PA-trisNTA-functionalized hydrogel by in situ 3D photoactivation by using mask lithography and laser scanning microscopy.

To improve the self-inactivation that results in a tight complex, we systematically investigated the influence of the linker length. Starting from PA-trisNTA **1** with an 11 amino acid linker between the trisNTA moiety and a pentahistidine tag, we decreased the linker length step-by-step from 11 to 3 amino acids (**1**–**5**). The Ala-Cys pair at the N terminus and the Anp in the center of the linker were kept constant (Scheme 1 B). The synthesis of **2**–**5** was performed by using the more cost effective racemic mixture of Anp. RP-C_{18}-HPLC purification of the compounds revealed distinct retention times for each diastereomer, termed (a) or (b) according to their elution time (see Figure S1 in the Supporting Information).

The PA-trisNTAs were fluorescently labeled with ATTO565 to allow the interaction with a protein of interest to be followed before and after illumination (366 nm, Xe/Hg lamp, 200 W, 20 min). The His-tagged maltose-binding protein (MBP-$H_{6/10}$) has proven to be an excellent and widespread model for trisNTA interaction.[15] The light-triggered interaction of PA-trisNTA with MBP-$H_{6/10}$ (5 μM each) was analyzed by size-exclusion chromatography (SEC; Figure 1 A). Improved autoinhibition was observed with decreasing linker length before photoactivation (Figure 1 B). We compared the self-inactivating potentials against MBP-H_6 and MBP-H_{10}, which have different binding affinities towards trisNTA (K_d of 2 nM and 0.1 nM in the case of MBP-H_6 and MBP-H_{10}, respectively).[11] For compound **4b**, an optimal autoinhibition with less than 0.7 % unspecific binding of MBP-H_{10} was detected at concentrations that were 50000-fold above the K_d value. The 5 amino acid linker of **4a**,**b** was found to be the critical threshold of the linker length. The fact that compounds **5a**,**b** with the 3 amino acid linker cannot block the binding of MBP-$H_{6/10}$ as optimally as **4a**,**b** with the 5 amino acid linker prior to photoactivation indicates that the backbone is too short to provide an optimal contact between the intramolecular histidine residues and the trisNTA moiety.

Notably, the autoinhibition also depends on the stereoconfiguration of the photocleavable Anp. To analyze this in more detail, the PA-trisNTAs **4a** and **4b** were synthesized de novo with enantiopure Anp. Interaction analysis revealed that (*S*)-Anp is favored over the *R* configuration (Figure 1 B). The binding of **4a**(*R*) and **4b**(*S*) to MBP-H_{10} before photoactivation varies from $<0.7\,\%$ for **4b**(*S*) to more than 15 % for **4a**(*R*). In conclusion, the 5 amino acid linker and the stereocenter of the photocleavable amino acid are critical in the formation of a tight, autoinhibited trisNTA–histidine complex.

After photoactivation, only 15 % of **1** bound to MBP-H_6 (Figure 1 B). We anticipated that the released intramolecular His-tag competed with the binding of His-tagged proteins. For this reason, we strategically introduced the Anp within the self-inactivating His-tag to reduce its multivalency after illumination. We know from previous studies that five histidine residues are required for autoinhibition and that the Anp does not interfere with the formation of a complex with the His-tag.[13c,16] The PA-trisNTAs **6** and **7** (both with the *S* configuration; Scheme 1 B) will release a sequence of three histidine residues after photocleavage, whereas two and three intramolecular histidine residues will remain in **6** and **7**, respectively. SEC analysis revealed distinct self-inactivation as well as protein interaction for **6** and **7** (Figure 1 B). Before photoactivation, MBP-H_{10} interacts with both, thus indicating that the trisNTA–histidine complexes are not sufficiently self-

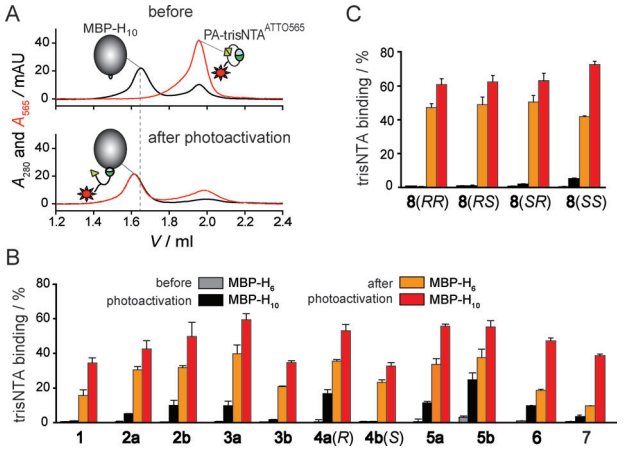

Figure 1. SEC analysis of in situ binding of PA-trisNTAs to His-tagged proteins before and after photoactivation. A) Size-exclusion chromatography of PA-trisNTA **8**(*RR*) and MBP-H_{10} before and after photoactivation. In situ interaction occurs only after activation with light. No interaction was observed in the presence of 100 mM imidazole (see Figure S3 in the Supporting Information). In all cases, the PA-trisNTAs were labeled with ATTO565. B) Autoinhibition and photoactivation properties of PA-trisNTAs with different peptidic linkers and intramolecular, photocleavable His-tags. C) Fine-tuned PA-trisNTAs with the optimal 5 amino acid linker and two photocleavable amino acids Anp in the *S* or *R* configuration. In all experiments, 5 μM of PA-trisNTA and MBP-$H_{6/10}$ was used.

inactivated. The His-tagged protein competed out 15% of the five intramolecular histidine residues in **6**, whereas compound **7** with six histidine residues showed 10% binding of MBP-H_{10}. Hence, the strength of the complex formed increases with the number of intramolecular histidine residues. Surface plasmon resonance (SPR) analyses showed that after photocleavage the remaining two and three intramolecular histidine residues of compounds **6** and **7**, respectively, were rebinding to the trisNTA and thereby interfering with the interaction with MBP-$H_{6/10}$ (see Figure S2 in the Supporting Information). This effect is more pronounced in **7** than **6** because of the larger number of intramolecular histidine residues. We anticipated that a synergistic effect between the linker length and the position of the Anp exists and that any remaining intramolecular histidine residues interfere with the formation of stable complexes with the His-tagged proteins.

Combining all these previous findings, we synthesized a final set of PA-trisNTAs with the optimal self-inactivating linker from **4a**,**b** and two photocleavable amino acids—one for photocleavage of the His-tag from the trisNTA and a second for photofragmentation of the His-tag itself (Scheme 1 A; **8**). The stereochemical influence of the Anp was also taken into account, since it has a major impact on the autoinhibition and photoactivation. Overall, four different diastereomeric PA-trisNTAs were synthesized and analyzed with regard to their interaction with His-tagged proteins (Figure 1 C). Before photoactivation, the PA-trisNTAs **8**(*RR*), **8**(*RS*), and **8**(*SR*) showed an improved autoinhibition with less than 1% nonspecific binding in the presence of MBP-H_{10} (**8** and MBP-H_{10}, 5 μM each). In comparison, **8**(*RR*) resulted in the formation of the tightest complex and the best self-inactivation properties (less than 0.3% unspecific binding). Even in the presence of 25-fold molar excess, **8**(*RR*) showed no detectable interaction with MBP-H_{10} (see Figure S3 in the Supporting Information). After photoactivation, all the PA-trisNTAs exhibited binding values ranging from 40% to 50% for MBP-H_6 and up to 60% for MBP-H_{10}.

The optimal behavior of **8**(*RR*) in terms of self-inactivation and light-triggered activation compared to **4b**(*S*) was further confirmed by SPR spectroscopy by using surface-immobilized PA-trisNTAs (Figure 2). The autoinhibition of

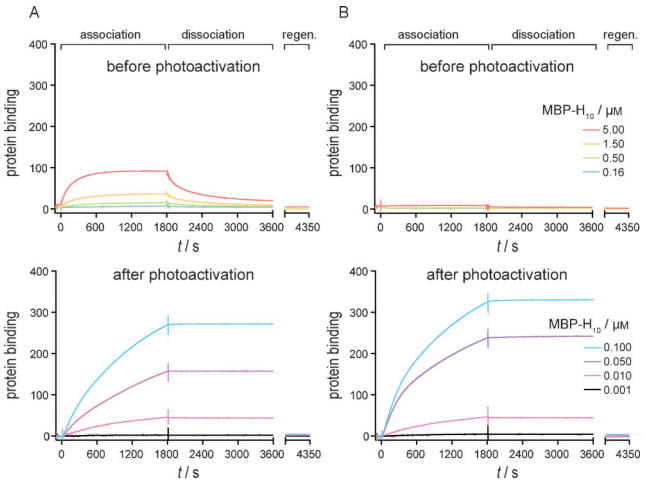

Figure 2. SPR analysis of the association and dissociation kinetics of MBP-H_{10} on surface-immobilized **4b**(*S*) (A) and **8**(*RR*) (B) before and after photoactivation. Complete self-inactivation of **8**(*RR*) is achieved even at 5 μM of MBP-H_{10}. After photoactivation, the protein binding is comparable to the immobilized free trisNTA (see Figure S4 in the Supporting Information). No interaction with His-tagged proteins was observed in the presence of EDTA or imidazole (regeneration), thus demonstrating the specificity of the interaction. The dissociation constants of the photoactivated PA-trisNTA **4b**(*S*) and **8**(*RR*) were determined to be 0.9 nM ($\chi^2 = 18$) and 1.3 nM ($\chi^2 = 124$), respectively. This is in good agreement with the free trisNTA ($K_d = 0.1$ nM).[15b]

both PA-trisNTAs was examined before photoactivation by increasing the concentration of MBP-H_{10} up to 5 μM (Figure 2, top). The interaction with MBP-H_{10} was investigated at 50-fold lower concentrations after photoactivation (Figure 2, bottom). In addition, we also analyzed the interaction with MBP-H_6 and free trisNTA as controls (see Figure S4 in the Supporting Information). The optimized **8**(*RR*) displayed full autoinhibition and no detectable binding even at the highest concentration of His-tagged proteins applied (> 1000 fold above the K_d value), whereas **4b**(*S*) showed some transient binding at increasing concentrations of MBP-H_{10}. After photoactivation, **8**(*RR*) and **4b**(*S*) showed a similar specific and high-affinity protein binding, reflected by very slow dissociation kinetics. This behavior is in good agreement with the free trisNTA (see Figure S4 in the Supporting Information). It is noteworthy that photocleaved His-tags were washed away, thereby resulting in 100% binding of MBP-$H_{6/10}$. In summary, the optimized PA-trisNTA **8**(*RR*) displays an excellent autoinhibition, since hardly any interaction was seen in its inactivated state in solution or at interfaces, even at extremely high local concentrations of His-

tagged proteins. Moreover, photodestruction of the cleaved His-tag by incorporation of a second Anp moiety leads to an increased photoactivation.

Hydrogels have found widespread applications because of their ease of fabrication and mechanical properties.[17] Neutral hydrogels composed of polyethylene glycol (PEG)[18] are very popular for biomedical applications, as they are much superior than hydrogels from natural sources (agarose, collagen, hyaluronic acid, etc.). Hybrid hydrogels with immobilized biomolecules, such as peptides or proteins, opened the opportunity to study cellular processes. Despite these advantages, the spatiotemporally controlled assembly of molecules in the hydrogel is still rare and only a few approaches exist.[12a,19] Here, we present a new method based on the newly designed PA-trisNTA for the in situ assembly of protein in hydrogels.

We prepared a hybrid matrix where the optimized PA-trisNTA **8**(*RR*) was linked to a maleimide polyvinyl alcohol (PVA) precursor (Scheme 1C). After polymerization, the functionalized hydrogel was photoactivated by mask photolithography (366 nm LED lamp, 185 mW cm^{-2}, 1 min), thereby generating a regular pattern of different dimensions. Visualization of the protein assembly in the hydrogel in the presence of MBP-$H_{10}^{ATTO565}$ (10 nM) by confocal laser-scanning microscopy (CLSM) demonstrated that the His-tagged proteins are organized only in photoactivated areas (Figure 3A; see Movie S1 in the Supporting Information). The high specificity of this process is reflected by an excellent signal-to-noise ratio.

In situ photoactivation provides the potential to drive reactions with high spatiotemporal control for microfabrication, tissue engineering, and receptor clustering. Patterns with different protein densities can be generated.[16,20] We therefore exploited the property of activating **8**(*RR*) with the 405 nm scanning laser of the CLSM (Figure 3B). Hence, regions of interest (ROIs) were photoactivated in the transparent hydrogel using a 40× objective with constant light intensity (25 mW) and various illumination times (1 to 12 scan iterations; 11.7 to 141.3 μs μm^{-1}). Gradually increasing protein densities were achieved with an excellent signal-to-noise ratio in the presence of MBP-$H_6^{ATTO488}$ (1.5 nM). No blurring of the edges was observed after 12 iterations and, hence, this modus was chosen for writing freely designed ROIs.

Protein arrays that permit simultaneous analysis of distinct properties avoid tedious repetitions and assure the same experimental conditions for all samples. Dual color experiments are an excellent proof of spatiotemporal activation and density control. Therefore, a combination of mask and in situ laser lithography was chosen for multiplexing (Figure 1C). First, **8**(*RR*)-functionalized hydrogel was photoactivated at 366 nm with a mask to write grids of MBP-$H_{10}^{ATTO565}$ (10 nM). Second, in situ patterning by the 405 nm scanning laser was used to consecutively anchor MBP-$H_6^{ATTO488}$ (1.5 nM) in selected photoactivated areas within the hybrid hydrogel (Figure 3C). The freely designed regions (snake) were written using a 40× objective, the optimal irradiation time of 141.3 μs μm^{-1}, and at a constant light intensity of 25 mW. The binding of MBP-$H_6^{ATTO488}$ was followed in real time (Figure 3C; see Movie S2 in the Supporting Information). The protein pattern can be perceived immediately after photoactivation, and well-defined structures with excellent signal-to-noise ratios were obtained after 10 to 15 min. A fast and efficient control of protein binding in the third dimension was thus realized by in situ photoactivation of PA-trisNTA **8**(*RR*). The high specificity and nanomolar affinity of the photoactivated trisNTA is also reflected by the excellent contrast. The reason why MBP-$H_6^{ATTO488}$ is also observed in the mask-patterned areas can be explained by the fact that the trisNTA binding sites are not saturated at this low concentration of His-tagged proteins and that the bound MBP-$H_{10}^{ATTO565}$ is bleached (see right edges of Figure 3D). Overall, this multiplexing approach enables sequential writing and readout of complex structures on a fast time scale.

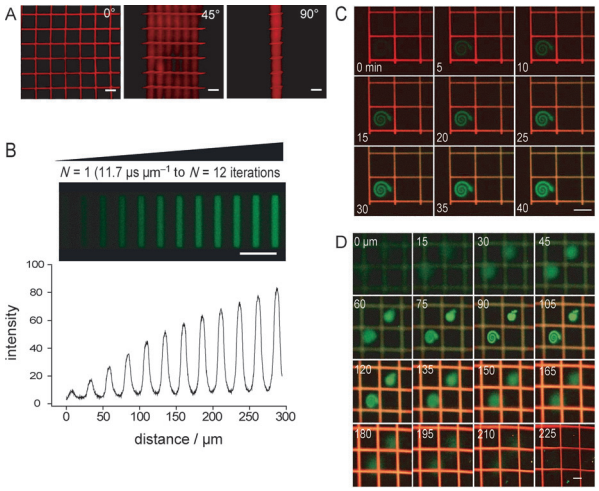

Figure 3. In situ protein assembly in four dimensions. A) Mask patterning at 366 nm and incubation with MBP-$H_{10}^{ATTO565}$ (10 nM). Photopatterning occurred through the entire volume of the hydrogel with high spatial resolution (see Movie S1 in the Supporting Information). B) Rectangular areas were iteratively photoactivated with the 405 nm laser to generate protein arrays with different densities and to determine the photoactivation time that gave the best signal-to-noise ratio. A good correlation between activation time and protein density was found. Notably, protein patterns can be observed even after one iteration (11.7 μs μm^{-1}). C) Freely designed regions of interest (ROI: snake) were generated by in situ photoactivation using a 405 nm scanning laser (see Movie S2 in the Supporting Information). 1.5 nM of MBP-$H_6^{ATTO488}$ was used. CLSM images were recorded every 5 min at ex/em 488/520 and 543/570 nm for MBP-$H_6^{ATTO488}$ and MBP-$H_{10}^{ATTO565}$, respectively. D) In situ photoactivation and protein assembly in three dimensions. The photoactivation in a small focal volume was demonstrated by the *z*-stacks, which were recorded every 15 μm (see Movie S3 in the Supporting Information). Scale bars correspond to 50 μm.

Defined *z*-stacks were recorded above and below the focal point where the ROI had been photoactivated. In situ photoactivation in the focal plane occurred at 0.5 μm resolution (*x*-*y*) and a *z* resolution of about 50 μm (Figure 3D; see Movie S3 in the Supporting Information). Images appear sharper in the focal plane, and are out of focus above and below. In summary, one-photon excitation allowed us to assemble proteins in four dimensions in a fast and simple way. Despite the lower resolution in the *z*-direction, this approach

mimics a multiphoton excitation, but with a standard laser-scanning microscope.[21] For even higher spatial resolution, in particular in the *z*-dimension, the potential of new amino acid derivatives in the PA-trisNTA that are accessible to multiphoton excitation is currently being investigated.

In conclusion, we have developed a series of fine-tuned PA-trisNTAs by systematic variation of the peptidic linker as well as the position and number of the photocleavable Anp. First, decreasing the linker length from 11 to 5 amino acids led to a well-matched autoinhibited complex. Second, the extra Anp within the His-tag prevented competition of the His-tag after photorelease. We also revealed that the stereochemistry of the photoactivatable amino acid plays a pivotal role in self-inactivation. The optimization of all these parameters converged in PA-trisNTA **8**(*RR*), which displays superior autoinhibition and photoactivation properties, as demonstrated by SEC and SPR analysis.

The fine-tuned PA-trisNTA **8**(*RR*) was used to build photoactivatable hybrid hydrogels for in situ assembly of protein. Different proteins can be photopatterned with excellent spatial resolution. Photoactivation proved to be tunable and extremely fast (ca. 140 $\mu s\,\mu m^{-1}$) and led to multiprotein arrays of different densities. Regions could be written with a scanning laser in the focal volume. The finely tuned PA-trisNTAs pave the way for several applications in chemical biology to track and control protein interaction. Since the His-tag is used almost in every life-sciences laboratory, our approach of photoactivatable trisNTAs is appealing for widespread applications that trigger cellular pathways in time and space.

Received: August 18, 2012
Revised: October 10, 2012

Keywords: 3D photopatterning · caged compounds · molecular recognition · photoactivation · protein assembly

[1] a) E. M. Sletten, C. R. Bertozzi, *Angew. Chem.* **2009**, *121*, 7108 – 7133; *Angew. Chem. Int. Ed.* **2009**, *48*, 6974 – 6998; b) J. A. Prescher, C. R. Bertozzi, *Nat. Chem. Biol.* **2005**, *1*, 13 – 21; c) K. M. Marks, G. P. Nolan, *Nat. Methods* **2006**, *3*, 591 – 596.

[2] D. Summerer, S. Chen, N. Wu, A. Deiters, J. W. Chin, P. G. Schultz, *Proc. Natl. Acad. Sci. USA* **2006**, *103*, 9785 – 9789.

[3] T. Fehrentz, M. Schonberger, D. Trauner, *Angew. Chem.* **2011**, *123*, 12362 – 12390; *Angew. Chem. Int. Ed.* **2011**, *50*, 12156 – 12182.

[4] a) D. Puliti, D. Warther, C. Orange, A. Specht, M. Goeldner, *Bioorg. Med. Chem.* **2011**, *19*, 1023 – 1029; b) S. Gug, F. Bolze, A. Specht, C. Bourgogne, M. Goeldner, J. F. Nicoud, *Angew. Chem.* **2008**, *120*, 9667 – 9671; *Angew. Chem. Int. Ed.* **2008**, *47*, 9525 – 9529.

[5] V. Gatterdam, T. Stoess, C. Menge, A. Heckel, R. Tampé, *Angew. Chem.* **2012**, *124*, 4027 – 4030; *Angew. Chem. Int. Ed.* **2012**, *51*, 3960 – 3963.

[6] N. Wu, A. Deiters, T. A. Cropp, D. King, P. G. Schultz, *J. Am. Chem. Soc.* **2004**, *126*, 14306 – 14307.

[7] a) H. M. Lee, D. R. Larson, D. S. Lawrence, *ACS Chem. Biol.* **2009**, *4*, 409 – 427; b) D. S. Lawrence, *Curr. Opin. Chem. Biol.* **2005**, *9*, 570 – 575; c) G. C. R. Ellis-Davies, *Nat. Methods* **2007**, *4*, 619 – 628; d) C. Brieke, F. Rohrbach, A. Gottschalk, G. Mayer, A. Heckel, *Angew. Chem.* **2012**, *124*, 8572 – 8604; *Angew. Chem. Int. Ed.* **2012**, *51*, 8446 – 8476; e) M. Goeldner, R. Givens, *Dynamic Studies in Biology*, Wiley-VCH, Weinheim, **2005**.

[8] a) G. V. Los, L. P. Encell, M. G. McDougall, D. D. Hartzell, N. Karassina, C. Zimprich, M. G. Wood, R. Learish, R. F. Ohane, M. Urh, D. Simpson, J. Mendez, K. Zimmerman, P. Otto, G. Vidugiris, J. Zhu, A. Darzins, D. H. Klaubert, R. F. Bulleit, K. V. Wood, *ACS Chem. Biol.* **2008**, *3*, 373 – 382; b) A. Keppler, S. Gendreizig, T. Gronemeyer, H. Pick, H. Vogel, K. Johnsson, *Nat. Biotechnol.* **2003**, *21*, 86 – 89; c) A. Gautier, A. Juillerat, C. Heinis, I. R. Correa, M. Kindermann, F. Beaufils, K. Johnsson, *Chem. Biol.* **2008**, *15*, 128 – 136; d) C. Uttamapinant, A. Tangpeerachaikul, S. Grecian, S. Clarke, U. Singh, P. Slade, K. R. Gee, A. Y. Ting, *Angew. Chem.* **2012**, *124*, 5954 – 5958; *Angew. Chem. Int. Ed.* **2012**, *51*, 5852 – 5856.

[9] B. A. Griffin, S. R. Adams, R. Y. Tsien, *Science* **1998**, *281*, 269 – 272.

[10] B. R. Hart, K. J. Shea, *Macromolecules* **2002**, *35*, 6192 – 6201.

[11] S. Lata, A. Reichel, R. Brock, R. Tampé, J. Piehler, *J. Am. Chem. Soc.* **2005**, *127*, 10205 – 10215.

[12] a) E. G. Guignet, R. Hovius, H. Vogel, *Nat. Biotechnol.* **2004**, *22*, 440 – 444; b) C. Orange, A. Specht, D. Puliti, E. Sakr, T. Furuta, B. Winsor, M. Goeldner, *Chem. Commun.* **2008**, 1217 – 1219.

[13] a) C. Grunwald, K. Schulze, G. Giannone, L. Cognet, B. Lounis, D. Choquet, R. Tampé, *J. Am. Chem. Soc.* **2011**, *133*, 8090 – 8093; b) G. Giannone, E. Hosy, F. Levet, A. Constals, K. Schulze, A. I. Sobolevsky, M. P. Rosconi, E. Gouaux, R. Tampé, D. Choquet, L. Cognet, *Biophys. J.* **2010**, *99*, 1303 – 1310; c) C. Grunwald, K. Schulze, A. Reichel, V. U. Weiss, D. Blaas, J. Piehler, K. H. Wiesmuller, R. Tampé, *Proc. Natl. Acad. Sci. USA* **2010**, *107*, 6146 – 6151.

[14] a) L. L. Parker, J. W. Kurutz, S. B. H. Kent, S. J. Kron, *Angew. Chem.* **2006**, *118*, 6470 – 6473; *Angew. Chem. Int. Ed.* **2006**, *45*, 6322 – 6325; b) M. Toebes, M. Coccoris, A. Bins, B. Rodenko, R. Gomez, N. J. Nieuwkoop, W. van de Kasteele, G. F. Rimmelzwaan, J. B. A. G. Haanen, H. Ovaa, T. N. M. Schumacher, *Nat. Med.* **2006**, *12*, 246 – 251.

[15] a) A. Tinazli, J. Tang, R. Valiokas, S. Picuric, S. Lata, J. Piehler, B. Liedberg, R. Tampé, *Chem. Eur. J.* **2005**, *11*, 5249 – 5259; b) S. Lata, J. Piehler, *Anal. Chem.* **2005**, *77*, 1096 – 1105.

[16] M. Bhagawati, S. Lata, R. Tampé, J. Piehler, *J. Am. Chem. Soc.* **2010**, *132*, 5932 – 5933.

[17] a) A. R. Hirst, B. Escuder, J. F. Miravet, D. K. Smith, *Angew. Chem.* **2008**, *120*, 8122 – 8139; *Angew. Chem. Int. Ed.* **2008**, *47*, 8002 – 8018; b) N. A. Peppas, J. Z. Hilt, A. Khademhosseini, R. Langer, *Adv. Mater.* **2006**, *18*, 1345 – 1360; c) I. Yoshimura, Y. Miyahara, N. Kasagi, H. Yamane, A. Ojida, I. Hamachi, *J. Am. Chem. Soc.* **2004**, *126*, 12204 – 12205.

[18] J. M. Zhu, *Biomaterials* **2010**, *31*, 4639 – 4656.

[19] a) C. A. DeForest, K. S. Anseth, *Angew. Chem.* **2012**, *124*, 1852 – 1855; *Angew. Chem. Int. Ed.* **2012**, *51*, 1816 – 1819; b) C. A. DeForest, K. S. Anseth, *Nat. Chem.* **2011**, *3*, 925 – 931; c) S. H. Lee, J. J. Moon, J. L. West, *Biomaterials* **2008**, *29*, 2962 – 2968; d) J. C. Hoffmann, J. L. West, *Soft Matter* **2010**, *6*, 5056 – 5063; e) K. A. Kilian, M. Mrksich, *Angew. Chem.* **2012**, *124*, 4975 – 4979; *Angew. Chem. Int. Ed.* **2012**, *51*, 4891 – 4895; f) Y. Luo, M. S. Shoichet, *Nat. Mater.* **2004**, *3*, 249 – 253; g) R. G. Wylie, S. Ahsan, Y. Aizawa, K. L. Maxwell, C. M. Morshead, M. S. Shoichet, *Nat. Mater.* **2011**, *10*, 799 – 806.

[20] M. Álvarez, J. M. Alonso, O. Filevich, M. Bhagawati, R. Etchenique, J. Piehler, A. del Campo, *Langmuir* **2011**, *27*, 2789 – 2795.

[21] M. S. Hahn, J. S. Miller, J. L. West, *Adv. Mater.* **2006**, *18*, 2679 – 2684.

